Low Temperature Dissociation of CO on Manganese Promoted Cobalt(poly)

Ryan A. Ciufo[†‡], Sungmin Han[†], Michael E. Floto[†], Graeme Henkeleman[†‡], C. Buddie Mullins*[†§]

[†] Department of Chemistry, University of Texas at Austin, Austin, Texas 78712, United States

[‡] The Oden Institute for Computational Engineering and Science, University of Texas at Austin, Austin, Texas 78712, United States

[§] McKetta Department of Chemical Engineering, Texas Materials Institute, Center for Electrochemistry, University of Texas at Austin, Austin, Texas 78712, United States

Abstract

The dissociation of CO is a vital step in the Fischer-Tropsch reaction for the production of alkanes and alkenes. The addition of Manganese to Cobalt in the form of MnO has historically been shown to tailor the selectivity of the Fischer Tropsch process. Here, we demonstrate that the addition of metallic Manganese to polycrystalline Cobalt promotes the dissociation of CO. Mn was deposited onto a Co(poly) foil in ultra-high vacuum, and CO adsorption was studied using King and Wells experiments and Reflection-Adsorption Infrared Spectroscopy at 100 K. The Mn promoted surfaces showed similar total CO uptake as compared to Co(poly), but the Mn/Co surfaces showed an increase in dissociated CO and respective decrease in molecular CO. Density Functional Theory calculations support experimental findings and show that Mn on Co(0001) stabilize dissociated $C_{(ad)}$ and $O_{(ad)}$ intermediates.

TOC Graphic

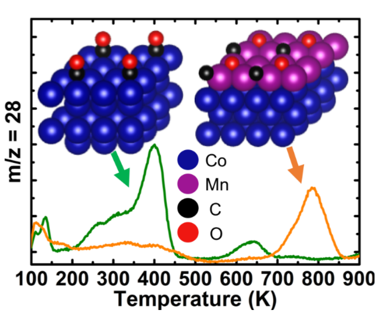

The Fischer-Tropsch (FT) process has been extensively studied for its use in producing hydrocarbons of various lengths from carbon monoxide and hydrogen gas.[1–3] Due to its tailorability, the FT process has shown promise to and continues to compete with the energy industry and petrochemical industry.[1,2,4] One area where FT shows much promise for growth is for the production of lower olefins. The production of lower olefins is one of the most important chemical processes in the world today for their use as chemical feedstocks for a number of industries. Most lower olefins are produced through cracking of a range of hydrocarbon feedstocks such as naptha, gas oil or light alkanes. Due to the energy cost of the cracking process and the limited petroleum reserves, there has been a push to develop alternative methods of deriving lower olefins. The Fischer-Tropsch to olefins process has shown the ability to break the traditional Anderson-Schultz-Flory (ASF) product distribution expected with Fischer Tropsch synthesis to produce lower olefins from syngas while limiting methane production.[5,6]

Among the few catalysts shown to break the ASF distribution are Manganese promoted Cobalt catalysts. Mn/Co systems have been shown to promote low chain olefin selectivity, C_{5+} selectivity, affinity for long chain alcohol synthesis, and increase overall intrinsic activity.[7–11] In addition to promoting Fischer Tropsch activity, $Co_xMn_{1-x}O$ mixtures were shown by Zhong *et al.* to form Co_2C nanoprisms under reaction conditions, which promoted the synthesis of lower olefins while limiting methane production to approximately 5%.[12] Importantly, in the above mentioned studies, the Mn was shown or believed to be in the form of Mn(II). However, theoretical work by Pederson, et al., suggested that metallic Mn alloyed with Co(111) could be responsible for some of the selectivity seen for their MnO promoted Fischer Tropsch catalysts.[7] In this letter, we report our investigation of the interaction of CO with metallic Mn promoted Cobalt polycrystalline surfaces by employing molecular beam techniques in ultra-high vacuum

(UHV). We show, using surface science techniques and Density Functional Theory (DFT), that the addition of metallic Mn as a promoter to Co facilitates dissociative adsorption of CO by stabilizing $C_{(ad)} + O_{(ad)}$ intermediates. These findings could provide insight into the unique Fischer Tropsch activity and selectivity of Mn/Co catalysts.

All experiments were performed in a supersonic molecular beam apparatus under ultrahigh vacuum conditions with a base pressure of 1 x 10^{-10} Torr, which has been described in detail in a previous paper.[13] In this study, various coverages of Mn were deposited onto a 10 x 15 x 0.7 mm Co(poly) substrate at 100 K and subsequently flashed to 900 K at 5 K/s to anneal the sample. All gas molecules were delivered via a neat molecular beam at room temperature (incidence energy of ~0.1 eV), which allows for the accurate control of the amount of adsorbed target molecules on the surface. Temperature programmed desorption (TPD) was adopted to analyze the gas phase species that evolved from the various Mn/Co surfaces. Reflection Adsorption Infrared Spectroscopy (RAIRS) was performed at 100 K to study surface intermediates. Prior to every experiment, the sample was cleaned with Ar^+ sputtering and

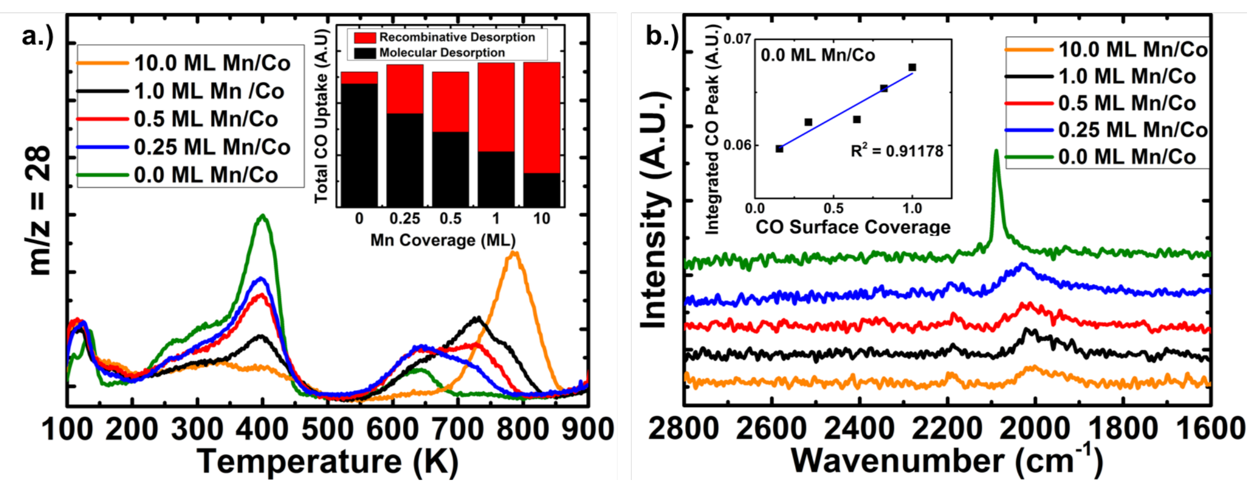

Figure 1. a.) CO TPD for various coverages of Mn on Co(poly) after CO K+W at 100 K. 1a, inset.) Total CO uptake from K+W at 100 K. Red depicts the fraction of molecular CO desorption. Black depicts the fraction of recombinative desorption b.) RAIRS performed at 100 K after K+W at 100 K for various coverages of Mn on Co(poly). 1b, inset.) Plot of area under molecular CO vibration peak for varying coverages of CO on 0.0 ML Mn/Co

annealing to 950 K. The cleanliness of the surface was verified with Auger Electron Spectroscopy (AES).

To study the uptake of CO on our surfaces, we performed King and Wells (K+W) experiments by impinging a molecule beam of CO on our each of our Mn/Co samples at 100 K. All K+W experiments were performed until surface saturation of CO uptake was detected. The total uptake during the K+W was quantified as the area under the CO mass spectrometer signal (Figure 1, inset. Figure S1). Following uptake experiments, CO TPD spectra were obtained (Figure 1a). As seen in Figure 1a, CO yields two major desorption features on the 0.0 ML Mn/Co surface (i.e., pure cobalt surface - green line), ~400 K and ~640 K. The feature near 400 K is the result of molecular CO desorption, while the feature near 640 K is the result of $C_{(ad)}$ + $O_{(ad)}$ recombinatively desorbing as CO.[14,15] It is seen that as the coverage of Mn is increased, there is an increase in intensity of the recombinative desorption feature and corresponding decrease in the molecular desorption feature. The recombinative desorption peak shifts to higher temperatures with increased Mn coverage (~775 K for 10 ML Mn/Co). These changes indicate an increased affinity for Mn covered surfaces to dissociate CO and suggest that intermediate $C_{(ad)}$ and $O_{(ad)}$ are stabilized on the Mn promoted surfaces. As the coverage of Mn on Co increases, new recombinative features appear at higher temperatures. For example, the 1.0 ML Mn/Co surface (Figure 1, black line) shows three distinct recombinative features at ~640 K, ~725 K, and ~775 K. We attribute the peak at ~640 K to recombinative desorption from cobalt sites.[14,15] For high coverages of Mn (~10 ML), a distinct feature is seen at ~775 K. We attribute this feature to recombinative desorption from predominantly Mn sites. Lastly, we attribute the feature seen at 725 K to mixed cobalt-manganese sites. Importantly, it is also seen that while CO dissociation is promoted with increasing Mn coverage, there is little change in the overall CO uptake for the Mn promoted surfaces as seen by the K+W (Figure 1a, inset).

To probe the nature of the interaction of adsorbed CO on our Mn/Co surfaces, RAIRS was performed at 100 K after K+W was performed at 100 K (Figure 1b). For a 0.0 ML Mn/Co surface, a sharp feature is seen at 2089 cm^{-1} corresponding to saturated linearly adsorbed molecular CO (green curve).[10,16] As Mn coverage increases, it is seen that the molecular CO vibration decreases in intensity, broadens, and shifts to lower wavenumbers, indicating decreased coverages of molecular CO which in turn have stronger binding to the surface.[17,18] This trend corresponds to the trend seen in Figure 1a, where increased Mn coverages show decreased molecular CO desorption. The decrease of the CO vibration further suggests that only a small fraction of CO is adsorbed molecularly on our Mn/Co surfaces at 100 K. It is important to note that no feature is seen for CO interactions with MnO (between 1700 – 1600 cm^{-1}),[10,19] suggesting that Mn exists as metallic Mn in our system.

While it is difficult to directly draw conclusions between IR spectra from different surfaces, the similarities between our samples allows for a qualitative comparison of molecular CO coverage.[20] We can develop a trend for the effect of CO coverage on IR intensity on 0.0 ML Mn/Co (Figure 1b, inset). We can then compare the trend from 0.0 ML Mn/Co to the trend seen from increasing Mn coverage on CO RAIRS intensity (Figure 1b). By varying exposure time from a molecular beam, we were able to controllably alter the surface coverage of CO on a 0.0 ML Mn/Co surface. RAIRS spectra were then acquired for the various coverages of CO on our surface. By plotting the integrated area under the molecular CO vibrational feature (from RAIRS) against CO surface coverage (Figure 1b, inset) determined on 0.0 ML Mn/Co, we see that area under the CO molecular vibration decreases with decreasing coverage. Notably, even small coverages of CO are detected by RAIRS and show molecular CO vibrations. For example, a CO surface coverage of ~ Θ = 0.15 gives a molecular CO feature that is within ~10% of the peak area observed for a CO saturated surface. Following this trend, we would also expect to observe molecularly adsorbed CO vibrations for high coverages of Mn/Co, which might be expected to have a small fraction of molecularly adsorbed CO and high fractions of dissociated CO. This pattern is in fact observed in Figure 1b where it can be seen that Mn covered surfaces show evidence of small RAIRS features due to molecularly adsorbed CO vibrations. This finding obviously suggests that at 100 K, adsorbed CO exists in both the molecular state and the dissociated state.

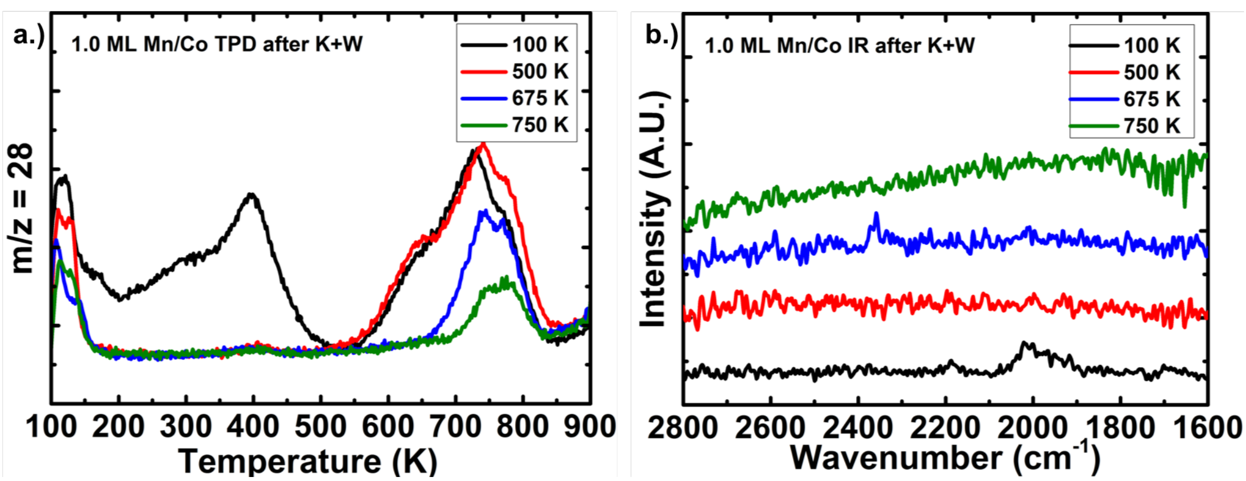

Figure 2. a.) CO TPD from 1.0 ML Mn/Co after CO K+W at various temperatures. b.) RAIRS at 100 K after CO K+W at various temperatures on 1.0 ML Mn/Co

To gain an understanding of the nature of the CO dissociation on our surfaces, we impinged a molecular beam of CO while holding the sample at various temperatures (Figure 2). In Figure 2a, TPD after impinging CO at 500 K (above the molecular desorption temperature but below the recombinative desorption temperature) shows a similar recombinative desorption feature when compared to the same experiment performed with the sample at 100 K. Following impinging at 500 K, the sample was cooled to 100 K and RAIRS was performed (Figure 2b, red curve). No molecular CO RAIRS feature is seen for the experiment performed at 500 K. The lack of molecular CO vibrations after exposure at 500 K and the similarity between the recombinative desorption features from the exposures at 100 K and 500 K further suggests that the desorption features seen above 650 K are from recombinative desorption rather than a strongly bound molecularly adsorbed CO entity. When the sample was held at 675 K and 750 K (Figure 2a blue and green curves, respectively), a decrease in the recombinative feature is observed due to the sample being held above the recombinative desorption temperature. At 675 K and 750 K, the recombinative desorption features at 640 K and 725 K decrease. As with the experiments described above at 500 K, after impinging CO onto the sample at 675 and 750 K, no molecular CO was observed with RAIRS (Figure 2b).

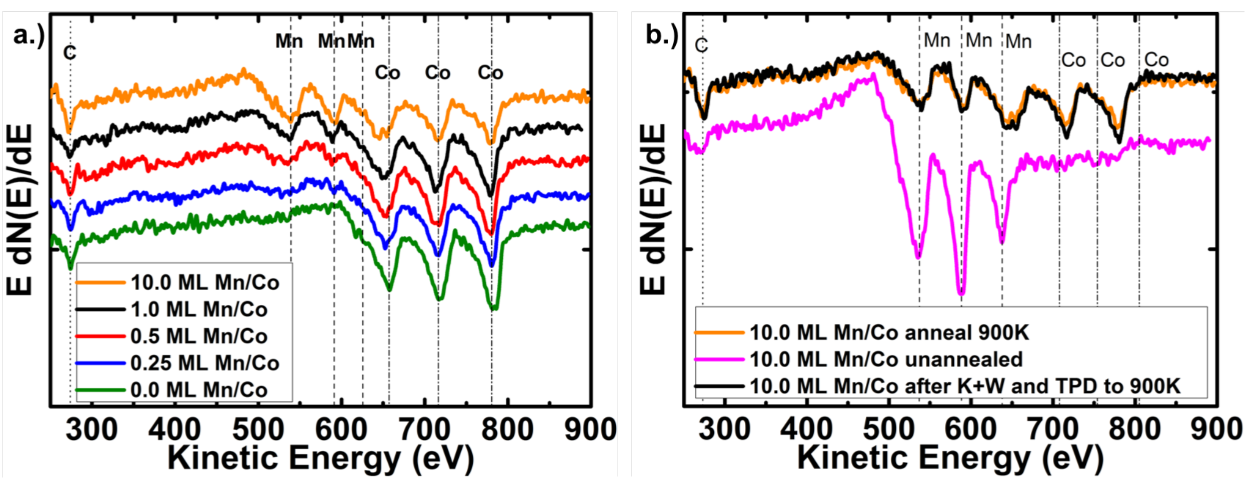

Figure 3. a.) AES spectra for various coverages of Mn on Co(poly). b.) Auger spectra before annealing, after annealing and after experiment for 10 ML Mn/Co

Auger electron spectroscopy was also employed to characterize our surface. As seen in Figure 3a, the AES spectra after evaporating Mn and annealing to 900 K at 5 K/s show Mn LMM features (540 eV, 594 eV, and 640 eV). The Mn features increase in intensity with increasing Mn coverages. Inversely, the Co LMM features (660 eV, 717 eV, and 783 eV) decrease with increasing Mn coverages. Figure 3b shows Auger spectra for a typical 10 ML Mn/Co surface annealed to 900 K (orange curve), for an unannealed 10 ML Mn/Co sample (magenta curve), and a post CO K+W at 100 K 10 ML Mn/Co annealed sample (black curve). It is seen that the freshly prepared, unannealed sample displays large Mn features and no Co LMM features. Upon annealing, the Co features reappear, and the Mn features decrease in intensity. The change in Mn:Co Auger intensity suggests that the Mn is migrating into the Co surface and alloying with the Co(poly), which aligns with previous work by Iijima, et al., which showed a high diffusivity for Mn in Co.[21,22] Following a K+W and a TPD experiment employing carbon monoxide, another Auger spectrum was taken of the 10 ML Mn/Co sample (Figure 3b, black line). The difference between the Auger before and after experiment is negligible, suggesting that the surface composition has not changed over the course of the experiment. Lastly, no oxygen features appear to be present in any of the Co/Mn spectra, further suggesting that Mn is in the metallic state and not oxidized.

To better understand the nature of the interaction between our surfaces and CO, we conducted DFT calculations. In contrast to earlier work by Pederson et. al,[7] we chose to study the HCP (0001) facet of Cobalt instead of the FCC (111) facet. HCP cobalt is the dominant phase present at low temperatures and the (0001) facet has the lowest surface energy.[23,24] Therefore, we expect HCP (0001) to be a predominant facet in our low temperature studies of Co(poly). Mn is found naturally in the I-43m space group, but for the purpose of this study was considered as a surface alloy with HCP Co.[25] For all Mn/Co models, CO adsorption was found to be most stable on three-fold hollow sites, in agreement with previous studies.[26] For the dissociated state, most stable structures were found with carbon bound to a hcp hollow site, and oxygen bound to a FCC hollow site, as seen previously for Co(0001) systems.[27,28] The systems were modelled as a 4-layer slab and (2x2) surface unit cell. The binding energies of molecular CO and dissociated $C_{(ad)}$ + $O_{(ad)}$ were calculated for all surfaces relative to gas phase CO and the respective clean surface. For 0.25 ML Mn/Co and 0.5 ML Mn/Co, there were 4 and 6 surface configurations possible, respectively (**Figure S2**). For the 0.25 and 0.5 ML systems, the mean binding energies were reported along with the standard deviation (Figure 4 blue and red curves).

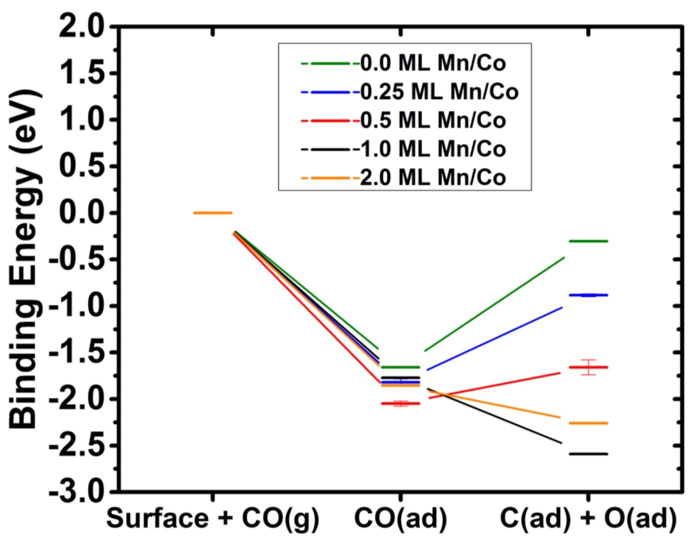

Figure 4. Schematic energy diagram of molecular CO adsorption and dissociated CO adsorption on Mn/Co surfaces.

As seen in Figure 4, an increase in molecular CO binding energy of ~0.2 eV was seen for all Mn/Co models compared to 0.0 ML Mn/Co with the exception of the 0.5 ML Mn/Co surface, which had a larger increase of ~0.35 eV. For the adsorption of dissociated $C_{(ad)}$ + $O_{(ad)}$, clean Co(0001) shows the weakest binding. As Mn coverage increases, the binding energy of $C_{(ad)}$ + $O_{(ad)}$ increases, with 1.0 ML Mn/Co having the strongest $C_{(ad)}$ + $O_{(ad)}$ binding energy of -2.59 eV. For 2.0 ML Mn/Co, the dissociated binding energy is ~ 0.35 eV weaker than on 1.0 ML Mn/Co. We believe that this decrease in $C_{(ad)}$ + $O_{(ad)}$ binding energy for 2.0 ML Mn/Co might be explained by unfavourability of large Mn ensembles to be in a HCP configuration. Evidence of this can be seen in Figure 3, where Mn readily alloys with Co. For both 1.0 ML and 2.0 ML Mn/Co, the binding of $C_{(ad)}$ + $O_{(ad)}$ is stronger than the binding of molecular CO. The observed increase of calculated binding energy of $C_{(ad)}$ + $O_{(ad)}$ on Mn promoted surfaces aligns with the higher recombinative desorption temperature seen experimentally (Figure 1a). Past work by Andreoni and Varma suggests that the boundary between molecular adsorption and dissociative adsorption of CO is mildly dependent on the molecular CO chemisorption energy and mostly dependent on the chemisorption energies of dissociated $C_{(ad)}$ and $O_{(ad)}$.[29] Our findings that $C_{(ad)}$ + $O_{(ad)}$ adsorb more strongly to Mn/Co surfaces align with our measurements showing that increased coverages of Mn on Co have higher fractions of dissociated CO. These results also suggest that CO is dissociatively adsorbing on our Mn promoted surfaces, which is in agreement with the RAIRS findings reported here (Figure 1b).

In summary, Mn annealed and alloyed with Co(poly) was seen to increase the dissociative adsorption of CO. Infrared spectroscopy showed decreased molecular CO vibrations on Mn covered surfaces, which is consistent with TPD findings from CO impingement experiments. By holding our sample at elevated temperatures above the molecular CO desorption temperature, we were able to show minimal change in recombinative desorption intensity, suggesting that dissociated CO states become populated at low temperature. Lastly, DFT calculations show that Mn covered Co(0001) models have increased molecular CO binding energy and increased $C_{(ad)}$ + $O_{(ad)}$ binding energy, which correlates with the presence of dissociated CO on our samples. These findings show that while MnO has historically been considered the active material for Mn/Co FT catalysts, metallic Mn can also be playing a role in CO dissociation.

Acknowledgements

We are thankful for the generous support of the Department of Energy Basic Energy Sciences (Grant DE-SC0018116 (C.B.M.) and Grant DE-SC0010576 (G.H.)) and the Welch Foundation (Grant F-1436 (C.B.M.) and Grant F-1841 (G.H.)). S.H. was partially supported by the Dorothy Banks Fellowship. Computational resources were provided by the Texas Advanced Computing Center and the National Energy Research Scientific Computing Center.

References

(1) Mahmoudi, H.; Mahmoudi, M.; Doustdar, O.; Jahangiri, H.; Tsolakis, A.; Gu, S.; LechWyszynski, M. A Review of Fischer Tropsch Synthesis Process, Mechanism, Surface Chemistry and Catalyst Formulation. *Biofuels Eng.* **2017**, *2* (1), 11–31. https://doi.org/10.1515/bfuel-2017-0002.

(2) Jahangiri, H.; Bennett, J.; Mahjoubi, P.; Wilson, K.; Gu, S. A Review of Advanced Catalyst Development for Fischer-Tropsch Synthesis of Hydrocarbons from Biomass Derived Syn-Gas. *Catal. Sci. Technol.* **2014**, *4* (8), 2210–2229. https://doi.org/10.1039/c4cy00327f.

(3) Yang, J.; Ma, W.; Chen, D.; Holmen, A.; Davis, B. H. Fischer-Tropsch Synthesis: A Review of the Effect of CO Conversion on Methane Selectivity. *Appl. Catal. A Gen.* **2014**, *470*, 250–260. https://doi.org/10.1016/j.apcata.2013.10.061.

(4) *Shell Investors' Handbook - Financial and Operational Information 2011-2015*; 2015.

(5) Torres Galvis, H. M.; De Jong, K. P. Catalysts for Production of Lower Olefins from Synthesis Gas: A Review. *ACS Catal.* **2013**, *3* (9), 2130–2149. https://doi.org/10.1021/cs4003436.

(6) Su, J.; Zhou, H.; Liu, S.; Wang, C.; Jiao, W.; Wang, Y.; Liu, C.; Ye, Y.; Zhang, L.; Zhao, Y.; et al. Syngas to Light Olefins Conversion with High Olefin/Paraffin Ratio Using ZnCrO x /AlPO-18 Bifunctional Catalysts. *Nat. Commun.* **2019**, *10* (1). https://doi.org/10.1038/s41467-019-09336-1.

(7) Pedersen, E. Ø.; Svenum, I. H.; Blekkan, E. A. Mn Promoted Co Catalysts for Fischer-Tropsch Production of Light Olefins – An Experimental and Theoretical Study. *J. Catal.* **2018**, *361*, 23–32. https://doi.org/10.1016/j.jcat.2018.02.011.

(8) Yang, Y.; Lin, T.; Qi, X.; Yu, F.; An, Y.; Li, Z.; Dai, Y.; Zhong, L.; Wang, H.; Sun, Y. Direct Synthesis of Long-Chain Alcohols from Syngas over CoMn Catalysts. *Appl. Catal. A Gen.* **2018**, *549* (September 2017), 179–187. https://doi.org/10.1016/j.apcata.2017.09.037.

(9) Feltes, T. E.; Espinosa-Alonso, L.; Smit, E. de; D'Souza, L.; Meyer, R. J.; Weckhuysen, B. M.; Regalbuto, J. R. Selective Adsorption of Manganese onto Cobalt for Optimized Mn/Co/TiO2 Fischer-Tropsch Catalysts. *J. Catal.* **2010**, *270* (1), 95–102. https://doi.org/10.1016/j.jcat.2009.12.012.

(10) Johnson, G. R.; Werner, S.; Bell, A. T. An Investigation into the Effects of Mn Promotion on the Activity and Selectivity of Co/SiO2 for Fischer-Tropsch Synthesis: Evidence for Enhanced CO Adsorption and Dissociation. *ACS Catal.* **2015**, *5* (10), 5888–5903. https://doi.org/10.1021/acscatal.5b01578.

(11) Morales, F.; Weckhuysen, B. M. Promotion Effects in Co-Based Fischer—Tropsch

Catalysis. *ChemInform* **2006**, *38* (2). https://doi.org/10.1002/chin.200702219.
(12) Zhong, L.; Yu, F.; An, Y.; Zhao, Y.; Sun, Y.; Li, Z.; Lin, T.; Lin, Y.; Qi, X.; Dai, Y.; et al. Cobalt Carbide Nanoprisms for Direct Production of Lower Olefins from Syngas. *Nature* **2016**, *538* (7623), 84–87. https://doi.org/10.1038/nature19786.
(13) Flaherty, D. W.; Hahn, N. T.; Ferrer, D.; Engstrom, T. R.; Tanaka, P. L.; Mullins, C. B. Growth and Characterization of High Surface Area Titanium Carbide. *J. Phys. Chem. C* **2009**, *113*, 12742–12752.
(14) Vaari, J.; Vaara, T.; Lahtinen, J.; Hautojarvi, P. Adsorption of CO on Mg-Promoted Co(Poly). *Appl. Surf. Sci.* **1994**, *81*, 289–297.
(15) Bardi, U.; Tiscione, P.; Rovina, G. Carbon Monoxide Dissociation on Polycrystalline Cobalt. *Appl. Surf. Sci.* **1986**, *27*, 299–317.
(16) Morales, F.; de Smit, E.; de Groot, F. M. F.; Visser, T.; Weckhuysen, B. M. Effects of Manganese Oxide Promoter on the CO and H2 Adsorption Properties of Titania-Supported Cobalt Fischer-Tropsch Catalysts. *J. Catal.* **2007**, *246* (1), 91–99. https://doi.org/10.1016/j.jcat.2006.11.014.
(17) Beitel, G. A.; Laskov, A.; Oosterbeek, H.; Kuipers, E. W. Polarization Modulation Infrared Reflection Absorption Spectroscopy of CO Adsorption on Co(0001) under a High-Pressure Regime. *J. Phys. Chem.* **1996**, *100* (30), 12494–12502. https://doi.org/10.1021/jp960045f.
(18) Rygh, L. E. S.; Ellestad, O. H.; Klaeboe, P.; Nielson, C. J. Infrared Study of CO Adsorbed on Co/γ-Al2O3 Based Fischer-Tropsch Catalysts; Semi-Empirical Calculations as a Tool for Vibrational Assignments. *Phys. Chem. Chem. Phys.* **2000**, *2* (8), 1835–1846. https://doi.org/10.1039/b000188k.
(19) Stevenson, S. A.; Lisitsyn, A.; Knözinger, H. Adsorption of Carbon Monoxide on Manganese-Promoted Rhodium/Silica Catalysts as Studied by Infrared Spectroscopy. *J. Phys. Chem.* **1990**, *94* (4), 1576–1581. https://doi.org/10.1021/j100367a066.
(20) Trenary, M. Reflection Absorption Infrared Spectroscopy and the Structure of Molecular Adsorbates on Metal Surfaces. *Annu. Rev. Phys. Chem.* **2000**, *51* (1), 381–403. https://doi.org/10.1146/annurev.physchem.51.1.381.
(21) Iijima, Y.; Hirano, K. I.; Tagijchi, O. Diffusion of Manganese in Cobalt and Cobalt-Manganese Alloys. *Philos. Mag.* **1977**, *35* (1), 229–244. https://doi.org/10.1080/14786437708235985.
(22) Attard, G.; Barnes, C. Auger Electron Spectroscopy. In *Surfaces*; 1998; pp 43–47.
(23) Ray, A. E.; Smith, S. R.; Scofield, J. D. Study of the Phase Transformation of Cobalt. *J. Phase Equilibria* **1991**, *12* (6), 644–647. https://doi.org/10.1007/BF02645161.
(24) Tran, R.; Xu, Z.; Radhakrishan, B.; Winston, D.; Sun, W.; Persson, K. A.; Ong, S. P. Data Descriptor: Surface Energies of Elemental Crystals. *Sci. Data* **2016**, *3*, 160080. https://doi.org/10.1038/cgt.2016.38.
(25) Gazzara, C. P.; Middleton, R. M.; Weiss, R. J.; Hall, E. O. A Refinement of the Parameters of α-Manganese. *Acta Crystallogr.* **1967**, *22* (6), 859–862. https://doi.org/10.1107/s0365110x67001689.
(26) Inderwildi, O. R.; Jenkins, S. J.; King, D. A. Fischer-Tropsch Mechanism Revisited: Alternative Pathways for the Production of Higher Hydrocarbons from Synthesis Gas. *J. Phys. Chem. C* **2008**, *112* (5), 1305–1307. https://doi.org/10.1021/jp710674q.
(27) Liu, J. X.; Su, H. Y.; Sun, D. P.; Zhang, B. Y.; Li, W. X. Crystallographic Dependence of CO Activation on Cobalt Catalysts: HCP versus FCC. *J. Am. Chem. Soc.* **2013**, *135* (44),

16284–16287. https://doi.org/10.1021/ja408521w.
(28) Li, B.; Zhang, Q.; Chen, L.; Cui, P.; Pan, X. Vacancy-Mediated Diffusion of Carbon in Cobalt and Its Influence on CO Activation. *Phys. Chem. Chem. Phys.* **2010**, *12* (28), 7848–7855. https://doi.org/10.1039/b925764k.
(29) Andreoni, W.; Varma, C. M. Binding and Dissociation of CO on Transition-Metal Surfaces. *Phys. Rev. B* **1981**, *23* (2), 437–444. https://doi.org/10.1103/PhysRevB.23.437.